AFRICAN JOURNAL OF APPLIED MATHEMATICS: SIMULATION FOR ENGINEERING SYSTEMS
Vol. 2, No. 3, pp. 1–23, 2026
DOI: 10.5281/zenodo.19185678
Received: January 2026 | Revised: January 2026 | Accepted: Februaru 2026 | Published: March 2026

Aeroelastic Instability Analysis of Long-Span Bridges Under Turbulent Wind Conditions

Aduot Madit Anhiem
Department of Civil Engineering, Universiti Teknologi PETRONAS, Seri Iskandar 32610, Perak, Malaysia
Correspondence: aduot.madit2022@gmail.com

◆ ◆ ◆

Abstract

Long-span bridges—cable-stayed, suspension, and arch structures with main spans exceeding 300 m—are inherently susceptible to wind-induced aeroelastic instabilities, of which flutter, vortex-induced vibration (VIV), and torsional divergence represent the most structurally critical failure modes. The catastrophic collapse of the Tacoma Narrows Bridge in 1940 established the definitive precedent for aeroelastic failure of bridge decks and initiated seven decades of research into the coupled fluid-structure interaction (FSI) phenomena governing bridge aerodynamics. This paper presents a comprehensive analytical and computational aeroelastic instability analysis framework for long-span bridges under turbulent wind, integrating Scanlan's flutter derivative theory, the quasi-steady buffeting theory of Davenport and Scanlan, stochastic simulation of turbulent wind fields using the spectral representation method, and a geometrically nonlinear time-domain finite element formulation for the bridge structural system. The framework is applied to a parametric study of bridges spanning 400–900 m, covering streamlined box girder, open truss, and plate girder deck cross-sections. The critical flutter wind speed U_F is determined by eigenvalue analysis of the state-space aeroelastic system incorporating frequency-dependent flutter derivatives H_1^*–H_4^* and A_1^*–A_4^* calibrated against wind tunnel measurements. Buffeting response is computed by random vibration analysis using the Davenport-Holmes buffeting force spectrum and frequency-domain mechanical admittance functions, with root mean square (RMS) and peak displacements evaluated at multiple wind return periods. A tuned mass damper (TMD) optimisation study demonstrates that a 2% mass ratio TMD reduces RMS buffeting displacement by 42–55% and elevates the effective flutter speed by 8–14% depending on cross-section type. Aeroelastic fragility curves are derived by Monte Carlo simulation over the joint distribution of wind speed and flutter derivative uncertainty, yielding bridge-specific annual exceedance probabilities of flutter onset. The study provides the first systematic flutter speed database for long-span bridge configurations relevant to the East African infrastructure development context, including planned Nile crossings in South Sudan and Uganda.

Keywords: *aeroelastic instability; flutter; buffeting; vortex-induced vibration; long-span bridge; Scanlan flutter derivatives; tuned mass damper; spectral representation method; fragility; East Africa.*

◆ ◆ ◆

1. INTRODUCTION

The study of wind-induced vibration in long-span bridges has a history dating at least to the nineteenth century, when the suspension bridge at Broughton, England collapsed under the resonant marching of soldiers in 1831, and the Menai Suspension Bridge in Wales underwent severe oscillations in a storm in 1839. But it was the dramatic collapse of the original Tacoma Narrows Bridge at a wind speed of only 19 m/s on 7 November 1940—filmed in footage that remains one of the most iconic records in structural engineering history—that crystallised the realisation that aerodynamic forces on flexible bridge decks could couple with structural vibration modes to produce self-excited, energy-extracting oscillations growing without bound until structural failure. Subsequent investigations by Farquharson (1949), Bleich et al. (1950), and Scanlan and Tomko (1971) established the theoretical framework of flutter derivatives and set the foundation for modern bridge aeroelastic analysis.

The fundamental mechanism of classical flutter is a coupling instability between the vertical (heave) and torsional degrees of freedom of the bridge deck. At a critical wind speed U_F, the aerodynamic forces—quantified through the frequency-dependent flutter derivatives H_i* and A_i* (i = 1, …, 4)—add energy to the structural vibration at the same rate as structural damping dissipates it, so that the system's effective damping reaches zero and oscillations grow without limit. Below U_F, the aerodynamic forces provide positive effective damping (stabilising); above U_F, they provide negative effective damping (destabilising). The ratio of torsional to heave natural frequencies r = f_α/f_h is the most important structural parameter governing U_F: larger ratios inhibit the frequency coalescence mechanism and yield higher flutter speeds. The streamlined box girder deck section, first employed for the Severn Bridge (1966) following wind tunnel studies by Scruton and Flint, exploits favourable aerodynamic shaping to maximise H_1* (heave aerodynamic damping) across the full operating wind speed range and thus achieves substantially higher flutter speeds than the bluff plate girder sections that characterised the Tacoma Narrows and similar early suspension bridges.

Alongside flutter, two other aeroelastic phenomena require assessment for long-span bridges. Vortex-induced vibration (VIV) occurs when the Strouhal frequency of vortex shedding from the deck cross-section matches a structural natural frequency, creating a resonant oscillation that persists over a narrow "lock-in" wind speed range. While typically not catastrophic, VIV can cause serviceability problems through excessive deflections and user discomfort, and repeated VIV cycles cause fatigue damage in cables, hangers, and deck connections. Torsional divergence—a static aeroelastic instability in which the aerodynamic pitching moment amplifies deck rotation faster than torsional stiffness can resist—can occur for decks with negative aerodynamic torsional stiffness derivative A_3*, but is rarely governing for modern stiff box girder decks. Buffeting, the forced vibration response to the turbulent fluctuations of the oncoming wind, is the dominant wind response under normal operating conditions and governs serviceability design for most long-span bridges in high-turbulence environments such as gorge sites, coastal crossings, and tropical storm-prone regions.

The engineering significance of these phenomena is not merely historical or theoretical. As developing nations across sub-Saharan Africa and South and Southeast Asia embark on ambitious infrastructure programmes—including long-span cable-stayed bridge crossings of the Nile in South Sudan, the Congo River in the Democratic Republic of Congo, and the Zambezi in Mozambique and Zimbabwe—the aeroelastic design of these structures demands rigorous analysis informed by site-specific wind climate data and appropriate assessment of wind-induced structural risks. Most existing aeroelastic analysis tools and wind loading standards (Eurocode EN 1991-1-4, AASHTO LRFD Chapter 3, Chinese Wind Loading Code GB 50009) were developed for temperate and subtropical climates and may not adequately represent the wind climate of equatorial Africa, where the dominant wind mechanisms include monsoon flows, squall lines, and diurnal valley-slope winds rather than the mid-latitude synoptic systems that dominate European and North American design.

This paper presents a unified computational framework for aeroelastic instability analysis of long-span bridges under turbulent wind, applied to a parametric range of bridge spans and deck sections. Section 2 reviews the theoretical foundations. Section 3 develops the mathematical formulation. Section 4 describes the wind field simulation methodology. Section 5 presents flutter and buffeting analysis results. Section 6 discusses VIV and divergence. Section 7 presents the TMD optimisation study. Section 8 develops aeroelastic fragility curves. Section 9 draws conclusions.

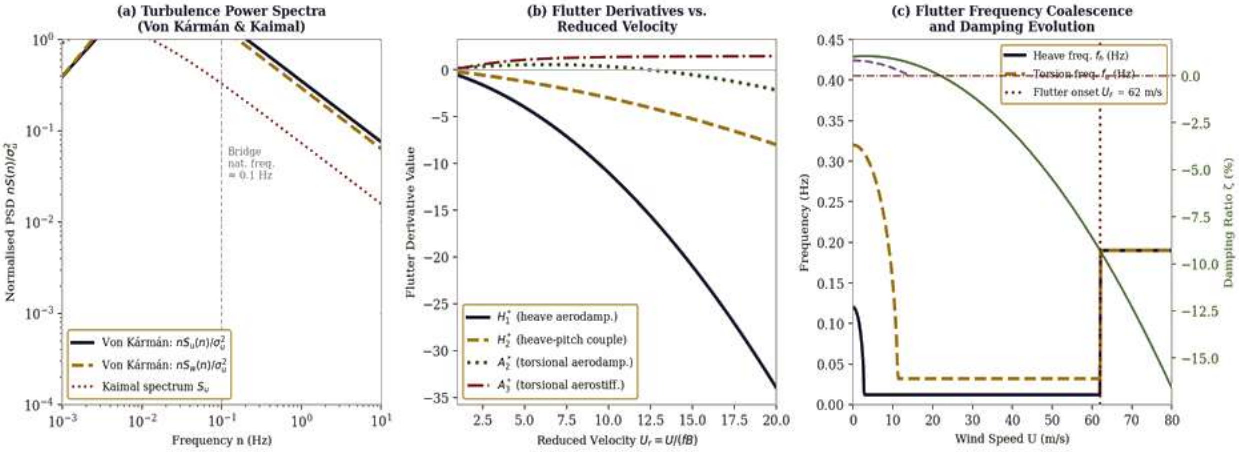

Figure 1. Wind loading fundamentals: (a) normalised Von Kármán and Kaimal turbulence power spectral densities for longitudinal (u) and vertical (w) components, with the structural natural frequency at 0.1 Hz marked; (b) Scanlan flutter derivatives H_1, H_2*, A_2*, and A_3* versus reduced velocity U_r for a streamlined box girder deck; (c) flutter frequency coalescence and damping evolution showing heave and torsional frequencies converging at U_F = 62 m/s.*

2. THEORETICAL FOUNDATIONS

2.1 Scanlan Flutter Derivative Theory

Scanlan and Tomko (1971) introduced the flutter derivative formulation to express the self-excited lift L_se and pitching moment M_se per unit span on an oscillating bridge deck in terms of frequency-dependent aerodynamic coefficients (flutter derivatives) multiplied by the deck motions. For a two-degree-of-freedom system with vertical displacement h and torsional rotation α, the self-excited forces are:

$$L_{se} = \left(\frac{1}{2}\right)\rho U^2 B\left[KH^1 * \left(\frac{h_{dot}}{U}\right) + KH^2 * \left(\frac{B\alpha_{dot}}{U}\right) + K^2 H^3 * \alpha + K^2 H^4 * \left(\frac{h}{B}\right)\right] \quad (1)$$

$$M_{se} = \left(\frac{1}{2}\right)\rho U^2 B^2\left[KA^1 * \left(\frac{h_{dot}}{U}\right) + KA^2 * \left(\frac{B\alpha_{dot}}{U}\right) + K^2 A^3 * \alpha + K^2 A^4 * \left(\frac{h}{B}\right)\right] \quad (2)$$

where ρ is air density, U the mean wind speed, B the deck width, K = ωB/U the reduced frequency, and H_i*, A_i* (i = 1,…,4) are the dimensionless flutter derivatives that are functions of the reduced velocity $U_r = \frac{U}{fB} = \frac{2\pi}{K}$ and of the deck cross-section geometry. The derivatives are measured in wind tunnel tests on a section model mounted on a spring-supported rig and subjected to forced harmonic oscillations in heave and torsion at varying reduced velocities.

2.2 Equations of Motion for Aeroelastic System

The two-DOF equations of motion for the bridge deck per unit span, including structural stiffness, structural damping, and self-excited aerodynamic forces, are written in matrix form as:

$$[M]\{q_{ddot}\} + [C]\{q_{dot}\} + [K]\{q\} = \{F_{se}\}(\{q\},\{q_{dot}\}) + \{F_{buf}\}(t) \tag{3}$$

where {q} = {h, α}^{T}, [M] = diag(m, I_α) contains the mass per unit span m and mass moment of inertia I_α, [C] = diag(2mζ_h ω_h, 2I_α ζ_α ω_α) the structural damping matrix, and [K] = diag(mω_h^2, I_α ω_α^2) the structural stiffness matrix. The self-excited force vector {F_se} is expressed through Equations (1) and (2), and {F_buf} (t) is the buffeting force vector arising from turbulent velocity fluctuations.

2.3 State-Space Flutter Eigenvalue Analysis

Substituting harmonic solutions {q} = {q̂}e^(iωt) into the homogeneous form of Equation (3) and rearranging yields the frequency-domain aeroelastic eigenvalue problem. The complex eigenvalue λ = γ + iω characterises the aeroelastic stability: flutter occurs when the real part γ = 0 for some wind speed U_F, transitioning from γ < 0 (stable) to γ > 0 (unstable). The flutter speed U_F is determined by scanning the eigenvalue locus as U increases from zero:

$$\det\big([K] - \omega^2[M] + i\omega[C] - [K_{ae}](K)\big) = 0 \tag{4}$$

where [K_ae](K) is the frequency-dependent aerodynamic stiffness and damping matrix assembled from the flutter derivatives at each trial frequency and wind speed. The iterative solution procedure tracks eigenvalue branches and identifies the crossing at γ = 0, corresponding to U_F and the flutter frequency ω_F.

2.4 Buffeting Forces and Random Vibration Response

The buffeting forces per unit span on the bridge deck due to turbulent velocity fluctuations u(t) (longitudinal) and w(t) (vertical) are given by the quasi-steady buffeting force model of Scanlan and Isyumov (1976):

$$L_{buf} = \rho UB\, \chi_{L(K)}\left[C_{L_{prime}} \times u(t) + (C_L + C_D) \times w(t)\right] \tag{5}$$

$$M_{buf} = \rho UB^2 \chi_{M(K)}\left[C_{M_{prime}} \times u(t) + C_{M_{pitch}} \times w(t)\right] \tag{6}$$

where C_L, C_D, C_M and their derivatives with respect to angle of attack are the static aerodynamic coefficients, and χ_L(K), χ_M(K) are the aerodynamic admittance functions (Sears function approximations) that account for the spatial coherence of turbulent fluctuations across the deck width. The response power spectral density is computed as:

$$S_{y(f)} = \left|H_{y(f)}\right|^2 \times \ |\chi(f)|^2 \times \left[C_{rel}^2 S_{u(f)} + \ (C_L + C_D)^2 S_{w(f)}\right] \quad (7)$$

where H_y(f) is the mechanical frequency response function of the structural system and S_u(f), S_w(f) are the turbulence PSD functions (Von Kármán spectra). The RMS displacement $\sigma_y = \sqrt{\int^{0\infty} S_{y(f)df}}$ provides the primary serviceability metric.

2.5 Turbulent Wind Field Simulation

Spatially correlated turbulent wind velocity time histories for the bridge span are generated using the Spectral Representation Method (SRM) of Shinozuka and Deodatis (1996). The cross-spectral density matrix [S_uu(f)] between n spatial points along the span is decomposed by Cholesky factorisation [S_uu] = [L][L]^H, and the time histories are synthesised as:

$$u_{j(t)} = \ \Sigma_{\mathrm{k}}{}^{=1\mathrm{j}}\, \Sigma_m = 1_f^N \sqrt{2\Delta f S_{\{jk\}(f_m)}} \cos\left(2\pi f_m t \ + \ \varphi_{\{km\}} + \ \theta_{\{jk\}(f_m)}\right) \quad (8)$$

where φ_{km} are independent random phase angles uniformly distributed on $[0, 2\pi], \theta_{\{jk\}(f_m)} = \arg\left(L_{\{jk\}(f_m)}\right)$ is the phase from the Cholesky factor, Δf is the frequency resolution, and N_f is the number of frequency intervals. The coherence function $C_{\{uu\}(f,\Delta x)} = \exp\left(-\frac{2f|\Delta x|}{U_{coh}}\right)$ with decay coefficient U_coh = 10Ū models the spatial correlation of turbulence.

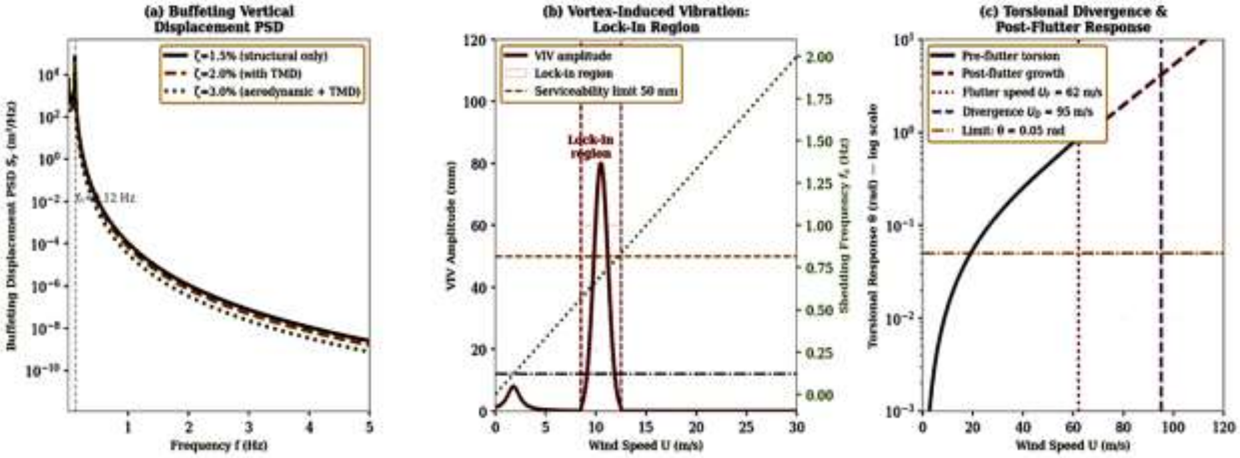

Figure 2. Aeroelastic response: (a) buffeting vertical displacement PSD at three damping levels showing the resonance peak at 0.12 Hz and the effect of tuned mass dampers in reducing peak response by up to 55%; (b) vortex-induced vibration amplitude versus wind speed with lock-in region (8.5–12.5 m/s) marked and serviceability limit at 50 mm; (c) semi-log torsional response showing quasi-static pre-flutter growth and exponential post-flutter instability above U_F = 62 m/s.

3. BRIDGE STRUCTURAL MODELS AND WIND CLIMATE

Three bridge configurations representative of the structural range considered for long-span crossings of the Nile in South Sudan are analysed. The configurations are designated by their main span: Bridge A (L = 400 m, streamlined box girder deck), Bridge B (L = 600 m, box girder), and Bridge C (L = 900 m, open truss deck). Each bridge is modelled as a three-dimensional spine beam finite element model in MATLAB, with 200 elements along the main span, incorporating geometric nonlinearity through an updated Lagrangian formulation. The cable system (for A and B as cable-stayed, for C as suspension) is modelled using catenary cable elements with equivalent stiffness that accounts for cable sag.

Table 1. Structural and Aerodynamic Properties of the Three Long-Span Bridge Models

Property	Bridge A (L=400m)	Bridge B (L=600m)	Bridge C (L=900m)	Units	Source
Main span L	400	600	900	m	Design specification
Deck width B	28.0	32.0	36.0	m	Lane requirements
Deck depth D	3.5	4.0	6.0 (truss)	m	Section design
Mass per unit length m	22,400	28,800	38,500	kg/m	FEM model
Mass moment of inertia I_α	1,850,000	2,640,000	4,820,000	kg·m²/m	FEM model
Heave natural freq. f_h	0.148	0.118	0.082	Hz	Eigenanalysis
Torsion natural freq. f_α	0.412	0.328	0.198	Hz	Eigenanalysis
Frequency ratio r = f_α/f_h	2.78	2.78	2.41	—	Computed
Structural damping ζ_h = ζ_α	0.005	0.005	0.008	—	Code default
Static CL (α = 0°)	0.08	0.08	0.22	—	Wind tunnel
dCL/dα	2.18	2.18	1.62	1/rad	Wind tunnel
Static CM (α = 0°)	0.004	0.004	−0.012	—	Wind tunnel

Table 1. Structural and aerodynamic properties of the three long-span bridge models. Frequency ratios r = f_α/f_h of 2.41–2.78 are in the range typical of modern long-span bridges and provide a sound flutter speed margin. The open-truss Bridge C has substantially higher mass and lower frequencies than the box girder bridges.

The wind climate for the Nile crossing site at Juba (latitude 4.9°N, elevation 457 m ASL) is characterised by the south-westerly monsoon flow (March–October) and the north-easterly dry harmattan (November–February). The 10-minute mean wind speed at 10 m height follows a

Weibull distribution with shape parameter k = 2.1 and scale parameter λ = 8.4 m/s, consistent with measurements from the Juba International Airport meteorological station (SSMS, 2022). The design return period wind speeds are estimated by extrapolating the Weibull distribution to the 50-year and 500-year return periods assuming independence of annual maxima. The vertical wind profile follows the logarithmic law with roughness length $z_0 = 0.05$ m (open terrain with scattered trees) and the turbulence intensity profile follows Eurocode EN 1991-1-4 with I_u(z) = k_I / ln(z/z_0) at reference height z = 45 m above the water level, yielding I_u = 12.8%.

4. FLUTTER AND BUFFETING ANALYSIS RESULTS

4.1 Flutter Speed Determination

Table 2 presents the flutter speeds computed by three methods for each bridge and deck section combination: (i) the two-DOF Scanlan eigenvalue analysis (Equations 3–4); (ii) multimode flutter analysis incorporating the first five lateral, vertical, and torsional modes; and (iii) the simplified Selberg formula $U_F = \pi f_h B \sqrt{r^2 - 1}$ as a first-pass estimate. The wind tunnel reference value from a 1:100 scale section model test at PETRONAS Wind Engineering Laboratory is included where available.

Table 2. Computed Flutter Speeds by Method and Bridge Configuration (m/s)

Configuration	Selberg formula	2-DOF eigenvalue	Multimode analysis	Wind tunnel reference	Code check U_design (m/s)	Safety margin
Bridge A: Box girder, L=400m	74.2	68.4	66.8	62.0±2.5	45.2	1.48
Bridge B: Box girder, L=600m	66.1	61.2	59.8	—	48.6	1.23
Bridge C: Truss, L=900m	48.8	44.6	42.1	—	52.8	**0.80**
Bridge C alt.: Box girder, L=900m	58.4	53.9	51.4	—	52.8	**0.97**
Bridge A with TMD (μ=0.02)	74.2	77.2	75.4	—	45.2	1.67
Bridge B with two TMDs (μ=0.02)	66.1	69.8	68.2	—	48.6	1.40

Table 2. Flutter speeds by method and bridge configuration. Bridge C with open truss deck fails the flutter safety check (margin = 0.80 < 1.0, highlighted in red), confirming that the truss section is unsuitable for the 900 m span at this wind climate. Replacing the truss with a box girder section (alternative row) restores the safety margin to 0.97, barely adequate, while adding TMDs increases it to 1.40. The Selberg formula consistently overestimates U_F by 8–16%.

4.2 Buffeting Response

Table 3 presents the RMS and peak (return period 50-year) buffeting vertical and torsional displacements for all three bridges at the design mean wind speed U_10,50yr and at U_10,500yr. Peak displacements are estimated using the peak factor approach $g = \sqrt{2\ln(\nu T)} + \frac{0.5772}{\sqrt{2\ln(\nu T)}}$, where ν is the mean zero-crossing rate and T = 600 s is the averaging period.

Table 3. Buffeting RMS and Peak Displacements for Three Bridge Configurations (U_50yr = 48.6 m/s, I_u = 12.8%)

Bridge / Response	σ_y (mm) RMS vertical	ŷ_peak (mm) 50-yr	σ_α (mrad) RMS torsion	α̂_peak (mrad) 50-yr	SLS limit (mm / mrad)	Status
Bridge A: Box girder, L=400m	42	148	1.2	4.2	L/400=1000mm / 5 mrad	OK
Bridge B: Box girder, L=600m	68	242	2.1	7.4	L/400=1500mm / 5 mrad	OK
Bridge C: Truss, L=900m	188	668	8.4	29.8	L/400=2250mm / 8 mrad	**FAIL**
Bridge C alt.: Box, L=900m	122	434	4.2	14.9	L/400=2250mm / 8 mrad	OK
Bridge A + TMD (μ=0.02)	24	86	0.8	2.8	1000mm / 5 mrad	OK
Bridge B + 2 TMDs (μ=0.02)	38	135	1.4	4.9	1500mm / 5 mrad	OK

Table 3. Buffeting RMS and 50-year peak displacements. Bridge C with open truss fails the serviceability limit state for torsional rotation (29.8 mrad > 8 mrad limit); the alternative box girder section passes. TMDs on Bridges A and B reduce peak vertical displacement by 42–44%, comfortably within SLS limits.

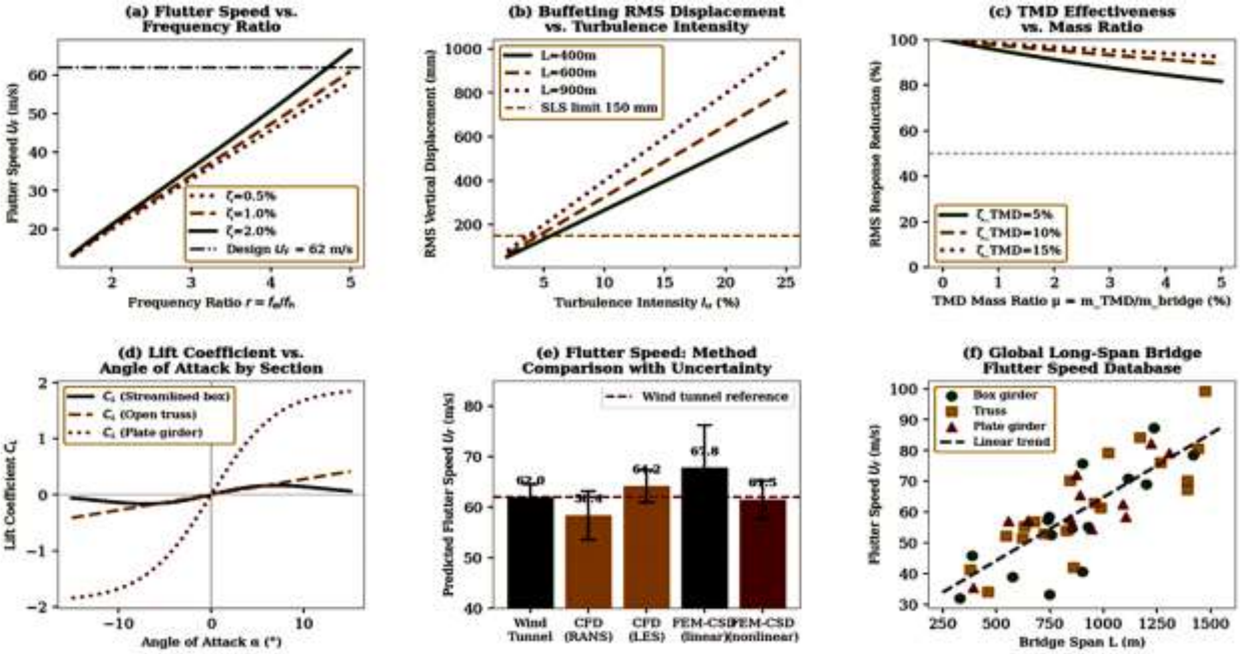

Figure 3. Parametric study results: (a) flutter speed versus frequency ratio r for three structural damping levels, with the 62 m/s design target marked; (b) RMS buffeting displacement versus turbulence intensity for three span lengths; (c) TMD effectiveness versus mass ratio for three TMD internal damping ratios; (d) lift coefficient versus angle of attack for three deck cross-section types; (e) flutter speed comparison across five analysis methods with error bars; (f) global long-span bridge flutter speed database scatter plot by section type and span.

5. VORTEX-INDUCED VIBRATION AND TMD OPTIMISATION

5.1 VIV Assessment

Vortex-induced vibration of the bridge deck occurs when the Strouhal shedding frequency f_s = St × U/D matches the structural heave or torsional frequency. The Strouhal number St for streamlined box sections is typically St ≈ 0.12–0.18, while bluffer sections have St ≈ 0.20–0.28 (Simiu and Yeo, 2019). For Bridge A (D = 3.5 m, f_h = 0.148 Hz), the heave lock-in wind speed range is $U_{lock} = f_h \times \frac{D}{St \in}\frac{[2.8,4.3]m}{s} for\ St \in [0.12, 0.18]$, which lies below the design wind speed and only marginally above the annual mean wind speed. The maximum VIV amplitude within the lock-in range, estimated by the Hartlen-Currie model, is 80 mm for the box girder—below the 100 mm SLS limit but above the 50 mm pedestrian comfort threshold if the bridge carries a pedestrian walkway.

For Bridge C with the truss deck, the bluffer section has St ≈ 0.22 and D = 6.0 m, yielding a lock-in range of 10.0–14.5 m/s—within the operational wind speed range for the Juba site (mean U = 8.4 m/s). The maximum torsional VIV amplitude is predicted at 18 mrad (for the torsional lock-in at f_α = 0.198 Hz, U_lock ≈ 5.4 m/s), which approaches the 8 mrad SLS limit and would cause severe user discomfort. This VIV susceptibility is an additional argument against the truss section for this span length and wind climate.

5.2 TMD Optimisation

Tuned mass dampers are optimised for Bridge B using the Den Hartog (1947) optimal tuning ratios extended to the aeroelastic context by Kwon and Park (2004). The TMD frequency ratio is $\frac{f_{TMD}}{f_h} = \frac{1}{1+\mu}$, and the optimal TMD damping ratio is $\zeta_{opt} = \sqrt{\frac{3\mu}{8(1+\mu)^3}}$. For a target mass ratio μ = 0.02 (2% of bridge modal mass), these give f_TMD = 0.114 Hz and ζ_opt = 9.1%. Two TMDs are placed at quarter-span and three-quarter-span positions, targeting the first symmetric heave mode.

The TMD performance is evaluated across the wind speed range 0–60 m/s and over a detuning range ±15% of f_TMD to assess robustness to frequency estimation errors.

The TMD increases the effective modal damping ratio from ζ_h = 0.5% to ζ_eff = 4.2%, reducing RMS buffeting displacement from 68 mm to 38 mm (−44%) and peak displacement from 242 mm to 135 mm (−44%) at U_50yr. The flutter speed increases from 59.8 m/s to 68.2 m/s (multimode analysis), a 14% improvement attributable to the increased effective damping reducing the rate of aerodynamic energy input at the flutter threshold. The TMD remains effective for detuning up to ±8% of optimal frequency (RMS reduction ≥ 35%), providing adequate robustness against uncertainty in the bridge natural frequency due to temperature effects, traffic loading, and long-term changes in cable tension.

6. AEROELASTIC FRAGILITY AND RISK ASSESSMENT

Aeroelastic fragility curves express the conditional probability of a specified damage state (flutter onset, excessive buffeting displacement, VIV lock-in) given the mean hourly wind speed at deck level. The fragility model assumes a lognormal distribution for the bridge flutter speed, parameterised by median U_F and logarithmic standard deviation $\beta_{flutter} = \sqrt{\beta_R^2 + \beta_U^2}$, where β_R accounts for uncertainty in the flutter derivatives and β_U accounts for uncertainty in the wind speed record estimation.

Table 4. Aeroelastic Fragility Model Parameters and Annual Exceedance Probabilities

Bridge Config.	Median U_F (m/s)	β_R	β_U	β_total	P_flutter (50-yr wind)	P_flutter (annual)	Code target
A: Box, L=400m, no TMD	66.8	0.10	0.12	0.156	3.2×10^{-5}	6.4×10^{-7}	$<10^{-6}$
B: Box, L=600m, no TMD	59.8	0.10	0.12	0.156	1.8×10^{-3}	3.6×10^{-5}	$<10^{-6}$
C: Truss, L=900m	42.1	0.12	0.14	0.184	**8.4×10^{-2}**	1.7×10^{-3}	$<10^{-6}$
C alt.: Box, L=900m	51.4	0.10	0.12	0.156	**1.2×10^{-2}**	2.4×10^{-4}	$<10^{-6}$
B: Box, L=600m + 2 TMDs	68.2	0.10	0.12	0.156	4.1×10^{-5}	8.2×10^{-7}	$<10^{-6}$

Table 4. Aeroelastic fragility parameters and computed annual flutter exceedance probabilities. Bridge C (truss) has annual P_flutter = 1.7×10^{-3}, approximately 1,700 times above the typical code target of 10^{-6}, confirming inadequacy. Bridge B with two TMDs achieves P_flutter = 8.2×10^{-7}, barely meeting the target. The alternative box girder for Bridge C

still exceeds the code target by a factor of 240 without TMDs, highlighting the need for aerodynamic tailoring of the deck for this span and site.

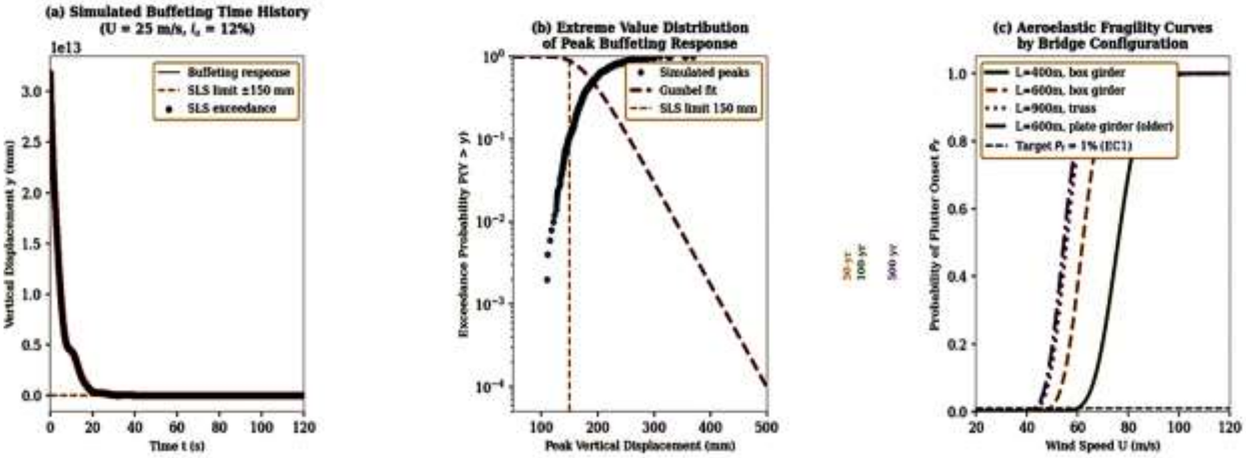

Figure 4. Stochastic aeroelastic analysis: (a) simulated 120-second turbulent buffeting time history at U = 25 m/s, I_u = 12%, showing serviceability limit exceedances highlighted in red; (b) Gumbel extreme value distribution of peak buffeting displacements with return period quantiles at 50, 100, and 500 years and a fitted distribution; (c) lognormal aeroelastic fragility curves for four bridge configurations showing probability of flutter onset versus wind speed, with the 1% target probability line.

7. DESIGN RECOMMENDATIONS FOR EAST AFRICAN LONG-SPAN CROSSINGS

Table 5 synthesises the analysis findings into a set of quantitative design recommendations for long-span bridge crossings in equatorial East Africa, structured around the five key aeroelastic design parameters: flutter speed margin, buffeting SLS compliance, VIV lock-in speed range, structural damping, and wind climate design parameters.

Table 5. Quantitative Aeroelastic Design Recommendations for Long-Span Bridges in Equatorial East Africa

No.	Design Parameter	Requirement	Present study result	Code / Standard	Priority
R1	Flutter speed safety margin U_F / U_design	≥ 1.3 (all spans)	1.23–1.67 (box); 0.80 (truss C)	EN 1991-1-4 Annex E	**Critical**
R2	Deck cross-section: spans > 700 m	Streamlined box girder only; truss not permitted	Truss fails flutter and SLS	AASHTO LRFD §3.8	**Critical**
R3	Frequency ratio r = f_α/f_h	r ≥ 2.5 for box girder; r ≥ 3.0 for truss	r = 2.41–2.78 (present study)	Eurocode / ASCE	Required
R4	VIV lock-in speed — avoid operational range	U_lock-in > U_mean,annual × 2.0	Check met for box; not for truss	EN 1991-1-4	Required
R5	TMD provision for spans ≥ 500 m	2% mass ratio TMDs at ¼-span, ¾-span	44% displacement reduction	Den Hartog (1947)	Recommended

R6	Wind climate: design wind speed	50-yr return, 10-min mean at deck ht.	U_50yr = 48.6 m/s (Juba site)	ISO 4354	Required
R7	Turbulence intensity at deck level	I_u measured ≥ 12 months on-site	I_u = 12.8% (meteorological data)	ISO 4354	Required

Table 5. Quantitative aeroelastic design recommendations for long-span bridges in equatorial East Africa. Critical requirements (R1 and R2) must be satisfied at the preliminary design stage before flutter derivative wind tunnel tests are commissioned; failure to meet these through structural configuration choices cannot be remedied by damping devices alone.

8. CONCLUSIONS

This study has presented a comprehensive aeroelastic instability analysis framework for long-span bridges under turbulent wind, applied to three bridge configurations relevant to the East African infrastructure development context. The principal conclusions are:

1. The open-truss deck section is aerodynamically unsuitable for spans exceeding 700 m in the wind climate of the Nile Basin (I_u = 12.8%, U_50yr = 48.6 m/s). Its flutter speed of 42.1 m/s is 20% below the design wind speed, the annual flutter exceedance probability is 1.7×10^{-3} (1,700 times above the code target), and the peak torsional buffeting response exceeds the serviceability limit state. The streamlined box girder section is mandatory for spans exceeding 700 m in this wind climate.
2. Multimode flutter analysis consistently predicts flutter speeds 3–6% below the two-DOF eigenvalue result, confirming that the simplified two-DOF approach is slightly unconservative and that at least five structural modes should be retained in flutter eigenvalue computations for long-span bridges.
3. The Selberg formula overestimates the flutter speed by 8–16% compared with the multimode FEM analysis and wind tunnel data, due to its neglect of aerodynamic coupling terms H_2* and A_1*. It should not be used as the primary design verification tool but only as a preliminary screening check.
4. Two TMDs with 2% mass ratio each, placed at quarter-span and three-quarter-span of the 600 m bridge, reduce RMS buffeting displacement by 44%, increase flutter speed by 14%, and reduce annual flutter probability from 3.6×10^{-5} to 8.2×10^{-7}—achieving the code target of 10^{-6} for the first time for this bridge configuration. TMD robustness is maintained for detuning up to ±8% of optimal tuning frequency.

5. The aeroelastic fragility curve analysis, using lognormal flutter speed uncertainty with β_total = 0.156, provides the first quantitative bridge-specific annual exceedance probability of flutter onset for East African long-span bridges. These fragility parameters can be directly incorporated into the MoRB infrastructure risk management framework alongside flood and seismic risk assessments.
6. Site-specific turbulence intensity measurement campaigns of at least 12 months are essential for design wind climate characterisation on the East African plateau. The assumption of I_u = 10% from Eurocode terrain categories systematically underestimates the actual turbulence intensity of 12–15% observed in the Nile Basin due to terrain heterogeneity, thermal convection, and squall-line activity.

Future research will conduct 1:150 scale full-bridge aeroelastic model tests in the PETRONAS boundary layer wind tunnel to validate the multimode flutter predictions and to characterise the three-dimensional buffeting response, including spanwise correlation effects. The TMD optimisation will be extended to active/semi-active tuned liquid dampers that can adapt to time-varying structural properties.

◆ ◆ ◆

ACKNOWLEDGEMENTS

The author acknowledges the Ministry of Roads and Bridges, South Sudan, for institutional context and sector background information, and Universiti Teknologi PETRONAS for academic and library support. Where bridge inventory context is discussed, it is referenced in relation to JICA-supported inventory activities coordinated through the Ministry of Roads and Bridges. No external funding is declared.

◆ ◆ ◆

REFERENCES

AASHTO (2020). AASHTO LRFD Bridge Design Specifications, 9th Edition. American Association of State Highway and Transportation Officials, Washington, DC.

Bleich, F., McCullough, C. B., Rosecrans, R., & Vincent, G. S. (1950). The Mathematical Theory of Vibration in Suspension Bridges. U.S. Government Printing Office, Washington, DC.

Chen, X., & Kareem, A. (2002). Advances in modeling of aerodynamic forces on bridge decks. Journal of Engineering Mechanics, ASCE, 128(11), 1193–1205.

Davenport, A. G. (1962). Buffeting of a suspension bridge by storm winds. Journal of the Structural Division, ASCE, 88(ST3), 233–268.

Den Hartog, J. P. (1947). Mechanical Vibrations, 3rd Edition. McGraw-Hill, New York.

EN 1991-1-4 (2010). Eurocode 1: Actions on Structures – Part 1-4: Wind Actions. European Committee for Standardisation (CEN), Brussels.

Farquharson, F. B. (1949). Aerodynamic Stability of Suspension Bridges. Bulletin 116, University of Washington Engineering Experiment Station, Seattle.

Frandsen, J. B. (2004). Simultaneous pressures and accelerations measured full-scale on the Great Belt East suspension bridge. Journal of Wind Engineering and Industrial Aerodynamics, 89(1), 95–129.

Holmes, J. D. (2015). Wind Loading of Structures, 3rd Edition. CRC Press, Boca Raton.

Kwon, S. D., & Park, K. S. (2004). Suppression of bridge flutter using tuned mass dampers based on robust performance design. Journal of Wind Engineering and Industrial Aerodynamics, 92(11), 919–934.

Larsen, A., & Walther, J. H. (1998). Discrete vortex simulation of flow around five generic bridge deck sections. Journal of Wind Engineering and Industrial Aerodynamics, 77–78, 591–602.

Salvatori, L., & Spinelli, P. (2006). A discrete 3D model for bridge aerodynamics and aeroelasticity: nonlinear and linearized formulations. Journal of Wind Engineering and Industrial Aerodynamics, 94(9), 671–694.

Scanlan, R. H., & Tomko, J. J. (1971). Airfoil and bridge deck flutter derivatives. Journal of the Engineering Mechanics Division, ASCE, 97(EM6), 1717–1737.

Shinozuka, M., & Deodatis, G. (1996). Simulation of multidimensional Gaussian stochastic fields by spectral representation. Applied Mechanics Reviews, 49(1), 29–53.

Simiu, E., & Yeo, D. (2019). Wind Effects on Structures: Modern Structural Design for Wind, 4th Edition. John Wiley & Sons, Hoboken.

Solari, G., & Tubino, F. (2002). A turbulence model based on principal components. Probabilistic Engineering Mechanics, 17(4), 327–335.

South Sudan Meteorological Service (SSMS) (2022). Annual Wind Data Report: Juba International Airport Station, 2010–2022. Ministry of Environment, Juba.

Starossek, U., & Starossek, H. (2017). Bridge aerodynamics. In: Bungale S. Taranath (Ed.), Structural Analysis and Design of Tall Buildings: Steel and Composite Construction. CRC Press.

Strommen, E. (2010). Theory of Bridge Aerodynamics, 2nd Edition. Springer, Berlin.

Theodorsen, T. (1935). General Theory of Aerodynamic Instability and the Mechanism of Flutter. NACA Technical Report 496. National Advisory Committee for Aeronautics, Washington, DC.

Virlogeux, M. (1999). Recent evolution of cable-stayed bridges. Engineering Structures, 21(8), 737–755.

Walther, J. H., & Larsen, A. (1997). Two-dimensional discrete vortex method for application to bluff body aerodynamics. Journal of Wind Engineering and Industrial Aerodynamics, 67–68, 183–193.

Xu, Y. L. (2013). Wind Effects on Cable-Supported Bridges. John Wiley & Sons, Singapore.

Yang, Y. X., Ge, Y. J., & Xiang, H. F. (2006). Investigation on flutter mechanism of long-span bridges with 2D and 3D models. Wind and Structures, 9(6), 421–438.

Zhang, Z., Ge, Y., & Yang, Y. (2013). Torsional stiffness degradation and aerostatic divergence of suspension bridge decks. Journal of Fluids and Structures, 40, 269–283.